NUMERICAL PREDICTION OF LEAN PREMIXED HYDROGEN DEFLAGRATIONS IN VENTED VESSELS

M. Khalil[1], A.D.L. Cheung[1], C.P.T. Groth[1], L. Ivan[2], and Z. Liang[2]

[1]University of Toronto Institute for Aerospace Studies
4925 Dufferin St., Toronto, Ontario, Canada, M3H 5T6

[2]Canadian Nuclear Laboratories
286 Plant Rd, Chalk River, Ontario, Canada, K0J 1J0

ABSTRACT

In water-cooled nuclear power plants, hydrogen gas can be generated by various mechanisms during an accident. In case combustion of the resulting hydrogen-air mixture within the facility occurs, existing containment structures may be compromised, and excessive radio-active material can be released to the environment. Thus, an improved understanding of the propagation of lean hydrogen deflagrations within buildings and structures is essential for the development of appropriate accident management strategies associated with these scenarios. Following the accident in Fukushima, Japan, the application of three-dimensional computational fluid dynamics methods to high-fidelity detailed analysis of hydrogen combustion processes in both closed and vented vessels has become more widespread. In this study, a recently developed large-eddy-simulation (LES) capability is applied to the prediction of lean premixed hydrogen deflagrations in vented vessels. The LES methodology makes use of a flamelet- or progress-variable-based combustion model coupled with an empirical burning velocity model (BVM), an anisotropic block-based adaptive mesh refinement (AMR) strategy, an accurate finite-volume numerical scheme, and a mesh-independent subfilter-scale (SFS) model. Several different vessel and vent sizes and configurations are considered herein. The LES predictions are compared to experimental data obtained from the Large-Scale Vented Combustion Test Facility (LSVCTF) of the Canadian Nuclear Laboratories (CNL), with both quiescent and turbulent initial conditions. Following descriptions of the LES models, LES results for both variable chamber sizes and single- and double-vent cases are presented to illustrate the capabilities of the proposed computational approach. In particular, the predicted time histories of pressure as well as the maximum overpressure achieved within the vessels and combustion compartments are compared to those from the LSVCTF experiments. The influences of the modelled ignition process, initial turbulence, and mesh resolution on the LES results are also discussed. The findings highlight the potential and limitations of the proposed LES approach for accurately describing lean premixed hydrogen deflagrations within vented vessels.

1.0 INTRODUCTION

As nuclear power has become more abundant in the 21^{st} century, so has the desire for significantly increased safety and accident prevention. While incidents such as Fukushima and Chernobyl are obviously highly undesirable, they can also provide unique opportunities to identify possible failure scenarios not previously considered. Consequently, many failure scenarios are now postulated as part of conceptual safety design studies for nuclear power plants, one being the failure of the reactor containment structure due to internal over-pressures [1, 2].

In water-cooled nuclear power plants, failure of the core cooling system, for whatever reason, can in some cases result in the oxidation of various metallic components by the water/steam present in the system and the even interaction of the concrete in the surrounding containment structures with a potentially molten reactor core, both of which can contribute to the formation of combustible hydrogen-air mixture within the reactor [3, 4]. As in the Fukushima incident, the combustion of such a mixture can result in structurally destructive over-pressures [1, 2] and the potential release of radio-active material. Various mitigation strategies for such failures have been devised for such failures including the use of pressure relief panels within multi-compartment containment facilities to inhibit pressure buildup due to steam formation and/or combustion. For this reason, an improved understanding of the propagation of lean hydrogen deflagrations within buildings

and structures is essential for the continued development of appropriate accident management strategies for nuclear power generation facilities.

Over the last few decades, many experiments have been performed to establish a fundamental understanding of vented deflagrations [5–7]. Furthermore, various empirical and analytical models have been developed for analyzing the effects of vented combustion involving various vessel geometries and mixture properties [6, 8–10], leading to the development of various engineering standards like the National Fire Protection Association (NFPA) 68 Standard [1, 2], which is widely used to guide the design of safety venting mechanisms for industrial applications. However, further experiments indicate that these standards have limited applicability, and may be ill-posed for use in some hydrogen deflagration scenarios [11, 12].

For the study of the containment of hydrogen deflagrations, reliable numerical simulation tools are somewhat more limited. The nuclear industry and safety regulators currently rely on lumped-parameter-type and more general-purpose, thermal-hydraulic, computational models and codes for numerical simulations and safety analyses related to hydrogen release and combustion [10, 13]. The combustion models adopted in these codes are generally rather simple and largely dependent on user-defined parameters to account for the presence of turbulence. There can be a high degree of uncertainty in the selection of suitable values for these parameters, particularly when considering new containment system designs. However, following the accident in Fukushima, Japan, the application of three-dimensional (3D) computational fluid dynamics (CFD) methods to high-fidelity detailed analysis of hydrogen combustion processes in both closed and vented vessels has become much more widespread. See, for example, the previous studies by Makarov *et al*. [14] and Makarov and Molkov [15].

In this study, a recently developed large-eddy-simulation (LES) capability is applied to the prediction of lean premixed hydrogen deflagrations in vented vessels. This LES framework was developed previously by Taylor *et al*. [16, 17] for modelling hydrogen combustion in closed vessels. The LES methodology makes use of a flamelet- or progress-variable-based combustion model coupled with an empirical burning velocity model (BVM), a block-based anisotropic adaptive mesh refinement (AMR) strategy, an accurate finite-volume numerical scheme, and a mesh-independent subfilter-scale (SFS) model. The LES framework is applied to the prediction of hydrogen combustion and the resulting pressure rise in containment vessels and vents of varying sizes and configurations. The predictions are also compared to experimental data obtained from the Large-Scale Vented Combustion Test Facility (LSVCTF) of the Canadian Nuclear Laboratories (CNL), with both quiescent and turbulent initial conditions [1, 2].

In what follows, descriptions of the LES modelling approaches used to simulate the premixed hydrogen reactive flows within the vented vessels and a summary of the LSVCTF experimental data sets are both given. The LES results for both variable chamber sizes and single- and double-vent geometries are then presented to illustrate the capabilities of the proposed computational approach. In particular, the predicted time histories of pressure as well as the maximum overpressure achieved within the vessels and combustion compartments are compared to those from the CNL LSVCTF experiments. The paper concludes with a summary of the findings from the present study.

2.0 LES METHOD FOR LEAN PREMIXED HYDROGEN DFLAGRATIONS

2.1 Favre-Filtered Navier-Stokes Equations

In the LES method adopted herein, the Favre-filtered form of the Navier-Stokes equations governing compressible flows of a thermally perfect reactive gaseous mixture is solved to describe the turbulent premixed combustion processes. Dufour, Soret and radiation effects are neglected. The partial differential equations governing the transport of the reactive mixture mass, momentum, energy, and species concentrations, for N_s

species can be written in tensor form as [16–20]

$$\frac{\partial \bar{\rho}}{\partial t} + \frac{\partial}{\partial x_i}\left(\bar{\rho}\tilde{u}_i\right) = 0\,, \tag{1}$$

$$\frac{\partial}{\partial t}\left(\bar{\rho}\tilde{u}_i\right) + \frac{\partial}{\partial x_j}\left[\bar{\rho}\tilde{u}_i\tilde{u}_j + \delta_{ij}\bar{p} - \left(\check{\tau}_{ij} + \sigma_{ij}\right)\right] = \bar{\rho}g_i\,, \tag{2}$$

$$\frac{\partial}{\partial t}\left(\bar{\rho}\tilde{E}\right) + \frac{\partial}{\partial x_i}\left[\bar{\rho}\tilde{u}_i\left(\tilde{E} + \frac{\bar{p}}{\bar{\rho}}\right) - \left(\check{\tau}_{ij} + \sigma_{ij}\right)\tilde{u}_j + \left(\check{q}_i + \theta_i\right)\right] = -\frac{\partial}{\partial x_i}\left[\sum_{\alpha=1}^{N_s}\Delta h^0_{\mathrm{f}_\alpha}\,\Gamma_{i,\alpha}\right] + \bar{\rho}\tilde{u}_i g_i\,, \tag{3}$$

$$\frac{\partial}{\partial t}\left(\bar{\rho}\tilde{Y}_n\right) + \frac{\partial}{\partial x_i}\left[\bar{\rho}\tilde{Y}_n\tilde{u}_i + \left(\check{\mathcal{J}}_{i,n} + \Gamma_{i,n}\right)\right] = \bar{\dot{\omega}}_n\,, \tag{4}$$

where ρ is the mixture density, u_i is the mixture velocity, p is the pressure, τ_{ij} is the fluid stress tensor, g_i is the acceleration vector due to gravity, E is the total energy of the mixture and its Favre-filtered value, $\tilde{E}$, is given by

$$\tilde{E} = \frac{1}{2}\tilde{u}_i\tilde{u}_i + \check{h}_\mathrm{s} - \frac{\bar{p}}{\bar{\rho}} + \sum_{\alpha=1}^{N_s}\Delta h^0_{\mathrm{f}_\alpha}\tilde{Y}_\alpha + k_\Delta\,, \tag{5}$$

q_i, is the heat flux vector, and Y_n are $J_{n,i}$ and are the mass fraction and mass flux relative to the mixture for species n, respectively. An overbar "–" represents a filtered quantity, a tilde " ˜ " represents a Favre-filtered quantity, and a chevron " ˇ " represents a quantity evaluated in terms of filtered quantities. Additionally, the LES sub-filter-scale (SFS) stress tensor, σ_{ij}, the SFS enthalpy flux, θ_i, and SFS species fluxes, $\Gamma_{i,n}$, for species n are defined as

$$\sigma_{ij} = -\bar{\rho}\left(\widetilde{u_i u_j} - \tilde{u}_i\tilde{u}_j\right)\,, \quad \theta_i = \bar{\rho}\left(\overline{h_\mathrm{s}u_i} - \check{h}_\mathrm{s}\tilde{u}_i\right)\,, \quad \Gamma_{i,n} = \bar{\rho}\left(\widetilde{Y_n u_i} - \tilde{Y}_n\tilde{u}_i\right)\,, \tag{6}$$

$k_\Delta = -\sigma_{ii}/2\bar{\rho}$ is the SFS turbulence kinetic energy, and $\bar{\dot{\omega}}_n$ is the filtered reaction rate for species n. Finally, in the above expressions, h_s is the sensible enthalpy, $\Delta h^0_{\mathrm{f}_n}$ is the heat of formation for species n, and δ_{ij} is the Kronecker delta function. Note that modelling of the SFS terms σ_{ij}, θ_i, and $\Gamma_{i,n}$ is required for closure of the preceding LES equation set.

2.2 Sub-Filter Scale Modelling

The Integral Length Scale Approximation (ILSA) model of Piomelli *et al*. [21, 22] is used herein to evaluate the SFS stress tensor, σ_{ij}. This models make use of a SFS eddy-viscosity approach, wherein the unclosed SFS stress tensor, which accounts for the effects of unresolved turbulence on the resolved LES flow field [23], takes the form

$$\sigma_{ij} - \frac{\delta_{ij}}{3}\sigma_{kk} = 2\bar{\rho}\nu_\mathrm{SFS}\left(\check{S}_{ij} - \frac{\delta_{ij}}{3}\check{S}_{kk}\right)\,. \tag{7}$$

where $\check{S}_{ij}$ is the resolved strain rate tensor and ν_SFS is the SFS turbulent viscosity. In standard Smagorinsky-type SFS models [24], the SFS viscosity is approximated using

$$\nu_\mathrm{SFS} = (C_s\Delta)^2|\check{S}|\,, \tag{8}$$

where Δ is the filter width and C_s is the so-called Smagorinsky constant (a value of $C_s = 0.18$ is commonly used). The filter width is defined to be proportional to the cubic root of the volume of the local computational cell. It is this link between the SFS viscosity and the mesh spacing that can cause issues when performing LES with non-uniform computational meshes, or sudden changes in mesh resolution [25], as is the case for the block-based AMR scheme employed herein [26–28]. For this reason, the ILSA model was proposed and developed specifically as a mesh independent SFS LES model by Piomelli *et al*. [21, 22] and is therefore adopted here. While still making use of an eddy viscosity approach, it differs in the evaluation of SFS turbulent viscosity, which instead is evaluated as

$$\nu_{\text{SFS}} = (C_k L_{\text{est}})^2 |\check{S}| \,, \tag{9}$$

where C_k is a model coefficient and L_{est} is an estimate of the integral length scale of the turbulence, which can be represented as

$$L_{\text{est}} = \frac{\langle\, K_{\text{res}} \,\rangle^{3/2}}{\langle\, \epsilon_{\text{tot}} \,\rangle} \,, \tag{10}$$

and where K_{res} is the resolved turbulent flow kinetic energy and ϵ_{tot} is the total (sum of resolved and SFS) turbulent dissipation rate. Local temporal averages of the resolved flow quantities with the local large-eddy turnover time as the averaging period, as represented by the angled brackets, "$\langle\ \ \rangle$", are used to evaluate the latter. The coefficient, C_k, is then found by solving locally a quartic equation and its value is dependent on a targeted level for the modelled turbulence relative to the total. In this way, the ILSA model remains active, even as the mesh is refined. Further details of the ILSA model can be found in Piomelli *et al*. [21, 22].

With the SFS stress tensor and turbulent viscosity defined, additional standard gradient transport assumptions are utilized here to model the SFS scalar fluxes, θ_i and $\Gamma_{i,n}$, in terms of the SFS eddy viscosity and SFS turbulent Prandtl and Schmidt numbers [18–20].

2.3 Flamelet-Based Combustion Model

In order to model the interaction between the chemical kinetics and turbulence and to specify the filtered reaction rates, $\bar{\dot{\omega}}_n$, for the premixed hydrogen flames of interest here, a standard flamelet-based combustion model is applied. In this approach, rather than solving directly for the species mass fractions, a reaction progress variable, c, with $c \in [0, 1]$ is introduced based on the mass fraction of the fuel (or gas temperature) in the burnt and unburnt states. A value of $c = 0$ corresponds to a mixture of fresh (pure) reactants and $c = 1$ to a mixture of burnt products. The treatment of the chemical kinetics is then reduced to solving a single Favre-filtered modelled transport equation for the reaction progress variable, which takes the form

$$\frac{\partial}{\partial t}\left(\bar{\rho}\tilde{c}\right) + \frac{\partial}{\partial x_i}\left(\bar{\rho}\tilde{c}\tilde{u}_i + \Gamma_{i,c}\right) = \rho_u s_{\text{T}} |\nabla \tilde{c}| = \rho_u s_{\text{L}} \Xi_\Delta |\nabla \tilde{c}| + S_{\text{ign}} \,, \tag{11}$$

where $\rho_u s_{\text{L}} \Xi_\Delta |\nabla \tilde{c}|$ represents the overall burning rate for the premixed flame, ρ_u is the density of the reactants, and s_{T} is the modelled turbulent flame speed. The latter is evaluated in terms of the product of the usual laminar flame speed, s_{L}, for the premixed mixture of fuel and oxidizer and the so-called flame wrinkling factor, Ξ_Δ, which accounts for flame wrinkling by the unresolved turbulence, preferential diffusion/thermodiffusive instabilities, and initial turbulence effects. The other source term appearing in Eq. (11), S_{ign}, is introduced here to represent the unsteady ignition of the premixed fuel and air by an external igniter. The modelling of this term is discussed in what follows below.

2.4 Burning Velocity Model (BVM)

The empirical-based burning velocity model (BVM) of Molkov and Bragin [29] is applied here to determine the combined filtered chemical reaction rate for the progress variable where the turbulent flame speed, s_{T}, is modelled as

$$s_{\mathrm{T}} = \Xi_{\Delta} s_{\mathrm{L}} = \Xi_{K} \Xi_{PD} \Xi_{F} \Xi_{AR} s_{L} e^{\left(\frac{u'}{s_T}\right)^2}, \tag{12}$$

where the flame wrinkling factor, Ξ_{Δ}, is the product of five factors: Ξ_{K} which models the effects of Karlovitz turbulence, Ξ_{PD} which models the effects of leading point flame propagation or preferential diffusion, Ξ_{F} which models flame surface fractal growth, Ξ_{AR} which incorporates the effect of the vessel's aspect ratio on flame acceleration, and the exponential term which represents the effects of the initial turbulence field with u' being the intensity of the initial turbulence. Refer to the previous work by Molkov and Bragin [29] for further details. The laminar flame speed is determined *a priori* using the Cantera software package [30] in conjunction with the chemical mechanism of Alekseev *et al*. [31] for hydrogen and air, which involves 9 chemical species and 20 reactions. To account for the changing pressure conditions within the vessel during the combustion process, an isentropic pressure correction is applied to adjust both the temperature and density of the reactants. The temperature correction is adjusted during the calculation of the flame speed in Cantera, and the density correction is performed during the evaluation of the burning rate using the BVM. The laminar flame speeds are produced for a set of hydrogen volume fractions (8%, 9%, 10%, 11%, and 12%), over a range of pressures from 100 kPa to 200 kPa, and fit into a linear function of pressure for use during simulation (one function per volume fraction). It should be noted that the combination of progress-variable flamelet and BVM models was shown previously to provide rather accurate LES predictions of hydrogen deflagrations in *closed* vessels for a range of conditions without any added tuning or modifications to improve agreement with experiment [16].

2.5 Empirical Ignition Model

The ignition process is modelled herein by introducing an empirically-based forcing term, S_{ign}, to the right-hand side of Eq. (11) which increases the value of the progress variable in a small volume of the domain, driving the value to a fully burned state with $\tilde{c} = 1$ within a specified period of time. The proposed forcing term is of the relaxation type and is taken to have the form

$$S_{\mathrm{ign}} = -\bar{\rho} \frac{(\tilde{c} - 1)}{\tau_{\mathrm{ign}}} f_{\mathrm{ign}}(t) \exp\left[-\left(\frac{6 \left\| \mathbf{x} - \mathbf{x}_{\mathrm{ign}} \right\|_2}{r_{\mathrm{ign}}} \right)^2 \right], \tag{13}$$

where τ_{ign} is the ignition time scale, r_{ign} is the ignition radius, $\mathbf{x}_{\mathrm{ign}}$ is the location of the forced ignition location, $f_{\mathrm{ign}}(t)$ is a cut-off function in time to limit the temporal duration of the ignition term. Appropriate values for τ_{ign} and r_{ign} were chosen to match experimental conditions for the vented deflagrations considered herein.

2.6 Finite-Volume Method

The governing LES equations outlined above are solved by applying a finite-volume spatial discretization procedure to each computational cell of a 3D multi-block body-fitted mesh composed of hexahedral volume elements. The finite-volume scheme makes use of a piecewise limited linear solution reconstruction and Riemann solver-based flux functions in the evaluation of the inviscid solution fluxes and, for the viscous fluxes, a centrally-weighted scheme is adopted. For this study, the approximate Riemann solver of Roe [32] is used in the inviscid flux evaluation. A standard second-order Runge-Kutta explicit time marching scheme

Fig. 1: Photograph and schematic diagram of the Large-Scale Vented Combustion Test Facility (LSVCTF) of the Canadian Nuclear Laboratories (CNL). The schematic diagram shows the vessel partitions, which are removed for the full-chamber tests.

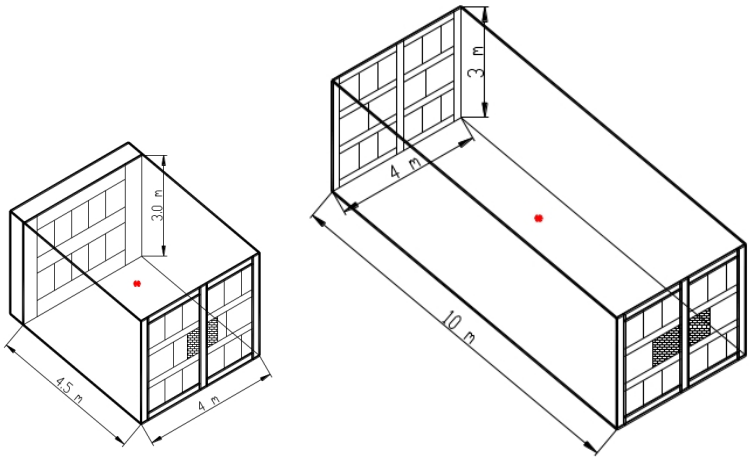

Fig. 2: Schematic diagrams of the LSVCTF half- and full-chamber vessel showing the vessel geometry and the positions of the vents.

is used to integrate the non-linear system of first-order ordinary differential equations resulting from the finite-volume discretization procedure and evolve the solution within each computational cell forward in time. Note that the proposed finite-volume methods was originally developed and to applied LES of reactive flows by Hernández-Pérez *et al*. [18, 19] and Shahbazian *et al*. [20].

2.7 Anisotropic Block-Based AMR

A flexible block-based hierarchical binary tree data structure is used in conjunction with the finite-volume spatial discretization procedure described above to allow automatic solution-directed anisotropic mesh adaptation of the body-fitted multi-block mesh. The block-based approach also readily facilitates highly scalable parallel implementations via domain decomposition. The AMR methodology was originally developed by Gao and Groth [33] for 3D steady flows, based on previous work for two-dimensional flows [34–36]. The current version of the algorithm makes use of the recently-developed anisotropic AMR scheme of Freret and Groth [26–28], based on the previous work of Williamschen and Groth [37]. The anisotropic AMR was most recently combined with the aforementioned finite-volume method and applied to LES of hydrogen deflagrations in closed vessels by Taylor *et al.* [16, 17].

3.0 LSVCTF EXPERIMENTS

The experiments performed by CNL using the LSVCTF were designed both to measure the development of overpressure resulting from lean hydrogen deflagrations within multi-compartment vented vessels and to study the effects of hydrogen concentration, vessel geometry, and vent size on the resulting over-pressure signatures [1, 2]. The experiments were performed using both full and half chamber configurations, with

Table 1: Summary of the LSVCTF full- and half-chamber experimental cases considered in the present study.

Case	Chamber Vol.	Vent Area	H_2 Fraction (Spec/Actual)	Initial Condition
S01-001	120 m^3	0.55 m^2	10%, 10%	Quiescent
S04-019	120 m^3	0.55 m^2	10%, 10%	Turbulent
FC018	57 m^3	0.35 m^2	8%, 7.8%	Quiescent
FC0823	57 m^3	0.35 m^2	9%, 9.2%	Turbulent
FC0807	57 m^3	0.55 m^2	9%, 9%	Turbulent

the full chamber having a volume of 120 m^3 (a rectangular cuboid 4 m wide, 3 m in height, and 10 m long) and the half chamber having a net equivalent volume of about 57 m^3 (again 4 m wide and 3 m in height with a length of about 4.75 m). A photograph and schematic diagram of the LSVCTF facility are given in Fig. 1 and schematic diagrams of the full- and half-chamber vessels are shown in Fig. 2. In the CNL experiments, the hydrogen concentrations were varied between 6–12% by volume and the vent sizes ranged from 0.22–0.55 m^2 for the half chamber configuration and from 0.35–1.1 m^2 for the full chamber. The vents were located towards the middle of the front wall of the vessel and mixing fans were used to achieve a homogeneous mixture. Both initially quiescent and turbulent conditions of the hydrogen-air mixtures were examined and, while the ignition was carried out at the centre of the chambers for the majority of cases, the influence of ignition location was also examined. During the turbulent tests, all of the mixing fans were turned on with a speed of 1,000 rpm. The maximum air speed in these cases was ~9 m/s at fans and ~4 m/s in the centre of the room. The volume-averaged flow velocity (U_{rms}) was found to be on the order of 1 m/s [1, 2]. For the quiescent or reduced turbulence experiments, the fans were shut off once a homogeneous mixture was achieved and ignition was delayed for a period of time to allow the decay of the turbulence field. In order to include the effects of initial turbulence in the simulations, an isotropic turbulence field generated using the method of Rogallo [38] and imposed on the computational grid. The turbulence was parametrized using turbulent kinetic energy, which is used to control the initial U_{rms} on the grid. and All of the experiments were performed with the hydrogen-air mixtures at ambient conditions (i.e., temperatures ranging from 18–25° C and pressures ranging from 96–100 kPa). Finally, scored thin aluminum sheets were used as vent diaphragms to control the initial pressure release with a burst overpressure about 1 kPa. Pressure transducer measurements were collected at various locations in the chamber and provide the mechanism for comparison with the LES predictions considered here. Please refer to the recent papers by Liang [1, 2] for a more complete description of the LSVCTF experiments.

For the present numerical study, a selected subset of the LSVCTF full- and half-chamber experimental cases are considered and summarized in Table 1. Two full-chamber cases are considered (S01-001, and S04-019) and three half-chamber cases are also considered (FC018, FC0823, and FC0807). For all of the cases considered, AMR was not used.

4.0 LES RESULTS

4.1 Full-Chamber Results

LES results are first considered for cases S01-001 and S04-019 outlined in Table 1, which constitute full-chamber, double vent LSVCTF configurations with a total vent area of 0.55 m^2, and 10% hydrogen concentration by volume. The primary difference between the two cases is the initial conditions, with the S01-001 corresponding to initially quiescent conditions and the S04-019 corresponding to turbulent conditions. Figure 3 illustrates multi-block mesh utilized for this study, which consisted of 380 computational

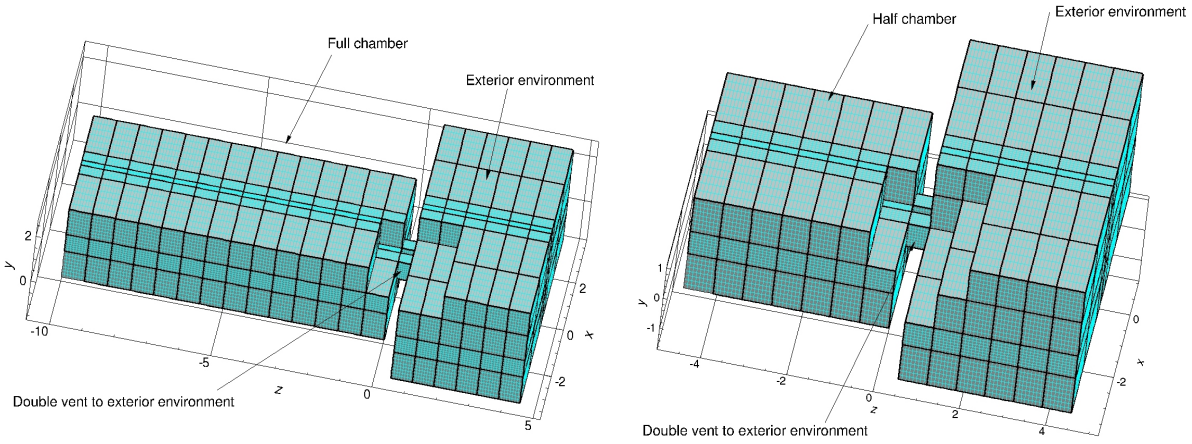

Fig. 3: 3D grids used in the LES of the full- (left) and half-chamber (right) vented vessels for LSVCTF cases S01-001 and S04-019 (full-chamber cases), as well as case FC0807 (half-chamber case). The mesh for the full-chamber vented vessel consists of 380, $6 \times 8 \times 8$, grid blocks for a total of 145,920 hexahedral computational cells. The coarse mesh for the full-chamber vented vessel consists of 275, $6 \times 8 \times 8$, grid blocks for a total of 105,600 hexahedral computational cells.

blocks, each containing 384 computational cells, resulting in a total of 145,920 cells. Two key LES model input parameters impacting the LES predictions for the LSVCTF cases are the ignition radius, r_{ign}, used in applying the simulated ignition source as described previously, and the specified level of initial turbulence as represented by u_{rms}, the initial root-mean-square averaged turbulence velocity as set by the initial turbulent kinetic energy per unit mass (TKE) on the grid. These two parameters were varied to replicate experimental conditions as closely as possible. In general, a small value of u_{rms} was used for the quiescent cases as compared to the turbulent cases, to account for the difference in the strength of the initial turbulence field.

Figure 4 depicts the predicted time histories of the over-pressure inside the chamber for the LES simulations of cases S01-001 and S04-019, and compares the predictions to the experimentally measured results. Note that the LES computations were performed until a pressure peak was reached. The left panel of Figure 4 provides the LES results for the quiescent case S01-001 with two sets of model parameters: $r_{\text{ign}} = 0.2$ m and $u_{\text{rms}} = 0.26$ m/s (TKE = 0.2 kJ/kg) and $r_{\text{ign}} = 0.2$ m and $u_{\text{rms}} = 0.36$ m/s (TKE = 0.5 kJ/kg). The comparisons for this quiescent case promising agreement between the LES and experimental results in terms of the magnitude of the maximum over-pressure. It also illustrates the sensitivity of the model to initial turbulence conditions, where a small difference in the average velocity field could have a significant impact on the predicted pressure behaviour. While tuning of the initial TKE can be used as a mechanism to match LES and experimental results more precisely in this case, it should be noted that the present simulations were performed on relatively coarse grids and, as such, the flame front and acoustic/pressure waves, which couple and can drive the burning rate in quiescent conditions [1], are not well resolved. As a result, the predicted pressure rise is relatively smooth compared to the more complex and oscillatory pressure behaviour observed in the experiments. For the relatively coarse considered in this first study, it is felt that the effects of acoustic coupling may be under estimated and tuning of u_{rms} would be just compensating for this fact.

The right panel of Figure 4 depicts the LES results obtained for case S04-019 with initially fully turbulent conditions. In this case, as the mixture is initially turbulent, the pressure rise is then driven by the turbulent acceleration of the premixed flame (the higher levels of turbulence leads to greater flame wrinkling and higher burning rates) and thus acoustic coupling has a diminished effect on pressure rise. As a consequence, it is felt that relatively coarse LES grids can potentially accurately reproduce the pressure rise measured in experiment. By using values of $r_{\text{ign}} = 0.4$ m and $u_{\text{rms}} = 4$ m/s for the ignition radius and turbulence intensity,

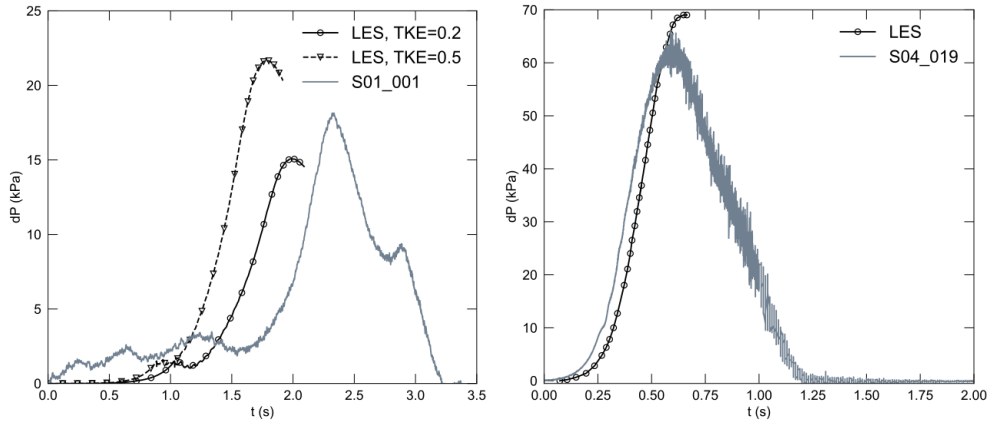

Fig. 4: LES results for full-chamber, double-vent, LSVCTF vented vessel cases with 10% hydrogen fuel-air mixture and an initially quiescent turbulent field, case S01-001 (left) and a fan-driven turbulent field, case S04-019 (right) showing comparisons of the predicted time histories of the vessel overpressure to the LSVCTF measurements.

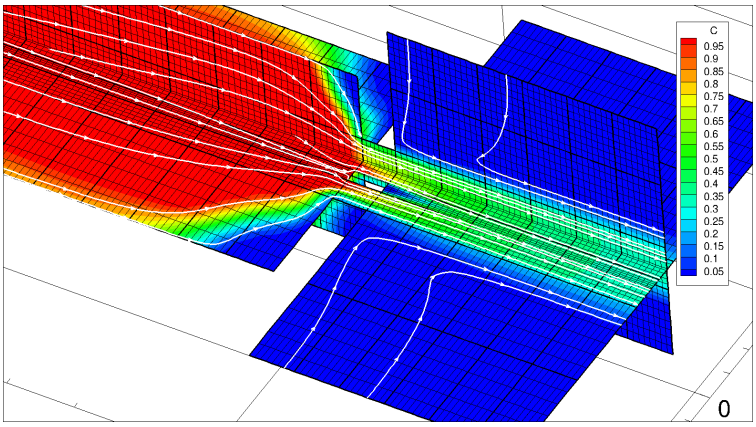

Fig. 5: LES results for full-chamber, double-vent, LSVCTF S04-019 vented vessel case with 10% hydrogen fuel-air mixture and fully turbulent initial conditions showing the instantaneous predicted distribution of the filtered progress variable, $\tilde{c}$, along with the predicted instantaneous streak lines at $t = 0.6$ s in the vicinity of the two vents.

respectively, where the latter roughly corresponds to measured levels in experiments prior to ignition, the LES results very accurately predict not only the maximum overpressure within the chamber, but the time at which the pressure peak occurs and the overall temporal variation of the pressure. Additionally, Figure 5 provides an illustration of the the instantaneous LES solutions of the reactive flow field within the vessel and venting to the atmosphere for case S04-019. The instantaneous distribution of the filtered progress variable, $\tilde{c}$, at $t = 0.6$ s, is depicted in the figure, along with the corresponding velocity streak-lines. Note that the escape of high-temperature products through both vent openings is clearly evident.

4.2 Half-Chamber Results

LES results are also considered for cases FC0018, FC0807 and FC0823 as outlined in Table 1. These cases correspond to half-chamber configurations with a total vent area of 0.35 m^2 and 0.55 m^2, respectively, and 8% and 9% hydrogen concentration. Case FC0018 is initially quiescent and cases FC0807 and FC0823 correspond to turbulent inital conditions. The right panel of Figure 3 provides the multi-block mesh utilized

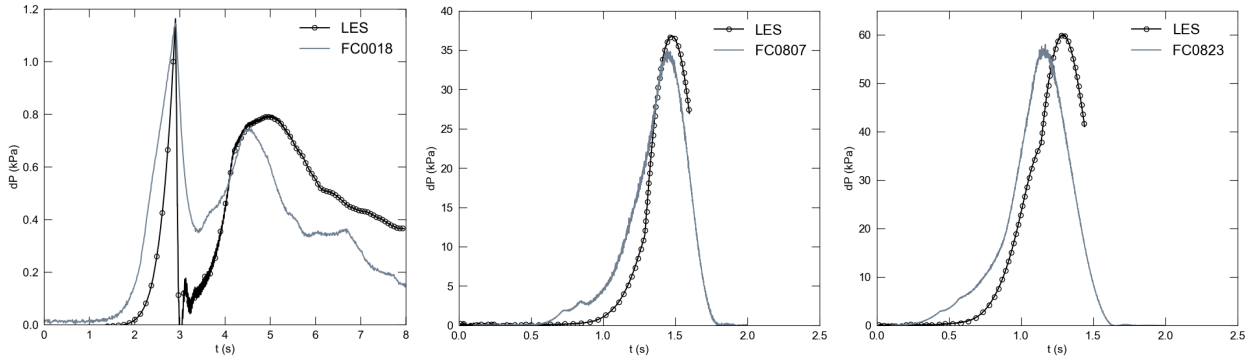

Fig. 6: LES results for the half-chamber LSVCTF vented vessel cases FC0018 (left), FC0807 (middle), and FC0823 (right) showing comparisons of the predicted time histories of the vessel overpressure to the LSVCTF measurements.

for case FC0807, which consisted of 275 computational blocks, each containing 384 computational cells, resulting in a total of 105,600 cells. The meshes for cases FC0018 and FC0823 was similar, except that the vents were reduced in cross section.

Figure 6 shows the predicted time predicted histories of overpressure inside the chamber for the half-chamber LES simulations and compares the predictions to the corresponding experimentally measured results. The simulation for the FC0018 case was performed with model parameters $r_{\text{ign}} = 0.2$ m and $u_{\text{rms}} = 0.26$ m/s, as they were found to provide a good match with experiments, while maintaining near quiescent initial conditions. The simulations for the FC0807 and FC0823 cases were performed with model parameters $r_{\text{ign}} = 0.21$ m and $u_{\text{rms}} = 2.5$ m/s. The latter were found to provide a good match with experiments while providing the correct levels of initial turbulence. The result of Figure 6 for all three half-chamber cases illustrate good agreement with experimental results, especially in terms of the magnitude and onset of the over-pressure peak. For case FC0018, due to the lower hydrogen concentration and quiescent conditions, the maximum overpressure is just 1.2 kPa. It can be seen that the initial pressure ramp-up until the vent opens just before 3 seconds is slightly faster than the experimental case, and this may be related to the chosen ignition radius, where a smaller radius may cause a slower pressure ramp up. It can also be noticed that following the vent opening, the pressure drops more rapidly than in the experiment. This may be attributed to a slower than expected burning rate, which could be a result of the relatively coarse LES mesh used in the simulation. For cases FC0807 and FC0823, the burning rate is increased by the higher levels of turbulence as is the pressure rise. It can be observed that the maximum magnitude and time onset of the pressure peak are again predicted rather accurately, despite the relatively coarse grid.

5.0 MODEL LIMITATIONS AND IMPROVEMENTS

The current study has established the proposed LES modelling framework as a strong baseline for potential usage as a computational tool for designing safer containment vessels. However, there are a few limitations that are worth considering. The first and most important limitation is the lack of treatment for mixture fraction. Currently, the reactants are assumed to be perfectly premixed with a single value for the mixture fraction. Distributed non-homogeneous initial stratification of the hydrogen and air with spatially varying values for the mixture fraction are possible in real-life conditions and cannot currently be taken into account. Secondly, the BVM combustion model adopted herein relies on the initial turbulence on the grid for the predicting turbulent burning rate; however, turbulent conditions can be quite different during the entire venting process. Accounting more directly for the instantaneous local turbulent conditions would obviously be important to consider.

6.0 CONCLUSIONS AND FUTURE RESEARCH

LES predictions of lean premixed hydrogen deflagrations in vented vessels have been presented and compared to available experimental data from the LSVCTF of CNL. The proposed LES framework makes use of a combination of progress-variable flamelet and BVM models for describing the turbulent burning and propagation of the premixed hydrogen flames and the ILSA SFS model for treatment of the unresolved turbulence. A finite-volume method is used to solve the governing Favre-filtered form of the governing partial differential equations. The potential of the proposed LES approach for accurately describing lean premixed hydrogen deflagrations in vented vessels has been demonstrated. The next steps will include modelling of the variation in the mixture fraction for exploring stratified mixtures as well as external combustion effects outside the vented chamber, the use of a combustion model that incorporates directly the instaneous local turbulent conditions in the flowfield, and exploring fully the application of AMR to refine the computational grids near flame fronts, more accurately predict acoustic coupling, and better capture the physics of the vented flows.

ACKNOWLEDGMENTS

The authors gratefully acknowledge the support from Canadian Nuclear Laboratories, under the auspices of the New Technology Initiatives Fund. Computational resources for performing all of the calculations reported herein were provided by the SciNet High Performance Computing Consortium at the University of Toronto and Compute/Calcul Canada through funding from the Canada Foundation for Innovation and the Province of Ontario, Canada.

References

[1] Z. Liang, Scaling effects of vented deflagrations for near lean flammability limit hydrogen-air mixtures in large scale rectangular volumes, Int. J. Hydrogen Energy 42 (10) (2017) 7089–7103.
[2] Z. Liang, Vented deflagrations for near lean flammability limit hydrogen-air mixtures in large scale inter-connected volumes, Int. J. Hydrogen Energy 42 (20) (2017) 14321–14331.
[3] F. Tanabe, Analyses of core melt and re-melt in the Fukushima Daiichi nuclear reactors, Journal of Nuclear Science and Technology 49 (1) (2012) 18–36.
[4] J. Yanez, M. Kuznetsov, A. Souto-Iglesias, An analysis of the hydrogen explosion in the Fukushima-Daiichi accident, Int. J. Hydrogen Energy 40 (25) (2015) 8261–8280.
[5] D. P. J. McCann, G. O. Thomas, D. H. Edwards, Gasdynamics of vented explosions. part I: Experimental studies, Combust. Flame 59 (1985) 233–250.
[6] D. P. J. McCann, G. O. Thomas, D. H. Edwards, Gasdynamics of vented explosions. part II: One-dimensional wave interaction model, Combust. Flame 60 (1) (1985) 63–70.
[7] M. G. Cooper, M. Fairweather, J. P. Tite, On the mechanisms of pressure generation in vented explosions, Combust. Flame 65 (1) (1986) 1–14.
[8] D. Bradley, A. Mitcheson, The venting of gaseous explosions in spherical vessels. I – theory, Combust. Flame 32 (1978) 221–236.
[9] D. Bradley, A. Mitcheson, The venting of gaseous explosions in spherical vessels. II – theory and experiment, Combustion and Flame 32 (1978) 237–255.
[10] D. Makarov, P. Hooker, M. Kuznetsov, V. Molkov, Deflagrations of localised homogeneous and inhomogeneous hydrogen-air mixtures in enclosures, Int. J. Hydrogen Energy 43 (2018) 9848–9869.
[11] F. Tamanini, Scaling parameters for vented gas and dust explosions, Journal of Loss Prevention in the Process Industries 14 (6) (2001) 455–461.
[12] V. V. Molkov, Accidental gaseous deflagrations: Modelling, scaling and mitigation, J. Phys. IV France 12 (7) (2002) 19–30.
[13] Z. Liang, C. K. Chan, M. Sonnenkalb, A. Bentaib, J. Malet, M. Sangiorgi, D. Gryffroy, S. Gyepi-Garbrah, J. Duspiva, T. Sevon, S. Kelm, E. A. Reinecke, Z. J. Xu, A. Cervone, H. Utsuno, A. Hotta, S. W. Hong, J. T. Kim, D. C. Visser, M. M. Stempniewicz, L. Kuriene, P. Prusinski, J. M. Martin-Valdepenas, W. Frid, P. Isaksson, J. Dreier, D. Paladino, D. Algama, A. Notafrancesco, A. Amri, M. Kissane, Status report on hydrogen management

and related computer codes, Organisation for Economic Co-Operation and Development, Nuclear Energy Agency (OECD/NEA) (2014).
[14] D. Makarov, F. Verbecke, V. Molkov, A. Kotchourko, A. Lelyakin, J. Yanez, D. Baraldi, M. Heitsch, A. Efimenko, A. Gavrikov, An intercomparison of CFD models to predict lean and non-uniform hydrogen mixture explosions, Int. J. Hydrogen Energy 35 (2010) 5754–5762.
[15] D. Makarov, V. Molkov, Numerical simulation of 10% hydrogen-air vented deflagration in a 120 m^3 enclosure, in: D. Bradley, G. Makhviladze, V. Molkov, P. Sunderland, F. Tamanini (Eds.), Proceedings of the Seventh International Seminar on Fire and Explosion Hazards (ISFEH7), Research Publishing, Singapore, 2013, pp. 975–984.
[16] C. R. Taylor, Mesh independent large-eddy simulation of hydrogen combustion in compromised nuclear facilities, Master's thesis, University of Toronto (September 2019).
[17] C. R. Taylor, C. P. T. Groth, Z. Liang, I. Lucian, Mesh-independent large-eddy simulation with anisotropic adaptive mesh refinement for hydrogen deflagration prediction in closed vessels, in: Proceedings of the 8th International Conference on Hydrogen Safety (ICHS 2019), Adelaide, Australia, September 24–26, 2019, p. Paper 123.
[18] F. E. Hernández-Pérez, F. T. C. Yuen, C. P. T. Groth, Ö. L. Gülder, LES of a laboratory-scale turbulent premixed Bunsen flame using FSD, PCM-FPI and thickened flame models, Proc. Combust. Inst. 33 (2011) 1365–1371.
[19] F. E. Hernández-Pérez, C. P. T. Groth, Ö. L. Gülder, Large-eddy simulation of lean hydrogen-methane turbulent premixed flames in the methane-dominated regime, Int. J. Hydrogen Energy 39 (2014) 7147–7157.
[20] N. Shahbazian, M. M. Salehi, C. P. T. Groth, Ö. L. Gülder, W. K. Bushe, Performance of conditional source-term estimation model for LES of turbulent premixed flames in thin reaction zones regime, Proc. Combust. Inst. 35 (2015) 1367–1375.
[21] U. Piomelli, A. Rouhi, B. J. Geurts, A grid-independent length scale for large eddy simulations, J. Fluid Mech. 766 (2015) 499–527.
[22] A. Rouhi, U. Piomelli, B. J. Geurts, Dynamic subfilter-scale stress model for large eddy simulations, Physical Review Fluids 1 (4) (2016) 044401–1–044401–26.
[23] U. Piomelli, Large-eddy simulation: Achievements and challenges, Prog. Aero. Sci. 35 (1999) 335–362.
[24] J. Smagorinski, General circulation experiments with te primitive equations. I: The basic experiment, Monthly Weather Review 91 (3) (1963) 99–165.
[25] S. B. Pope, Ten questions concerning the large-eddy simulation of turbulent flows, New Journal of Physics 6 (35) (2004) 1–24.
[26] L. Freret, C. P. T. Groth, Anisotropic non-uniform block-based adaptive mesh refinement for three-dimensional inviscid and viscous flows, Paper 2015-2613, AIAA (June 2015).
[27] L. Freret, L. Ivan, H. De Sterck, C. P. T. Groth, A high-order finite-volume method with anisotropic AMR for ideal MHD flows, Paper 2017-0845, AIAA (January 2017).
[28] L. Freret, L. Ivan, H. De Sterck, C. P. T. Groth, High-order finite-volume method with block-based AMR for magnetohydrodynamics flows, J. Sci. Comput. 79 (1) (2019) 176—208.
[29] V. Molkov, M. Bragin, Hydrogen-air deflagrations: Vent sizing correlation for low-strength equipment and buildings, Int. J. Hydrogen Energy 40 (2) (2015) 1256–1266.
[30] California Institute of Technology, CANTERA Release 1.8, http://code.google.com/p/cantera (2009).
[31] V. A. Alekseev, M. Christensen, A. A. Konnov, The effect of temperature on the adiabatic burning velocities of diluted hydrogen flames: A kinetic study using an updated mechanism, Combust. Flame 162 (5) (2015) 1884–1898.
[32] P. L. Roe, Approximate Riemann solvers, parameter vectors, and difference schemes, J. Comput. Phys. 43 (1981) 357–372.
[33] X. Gao, C. P. T. Groth, A parallel solution-adaptive method for three-dimensional turbulent non-premixed combusting flows, J. Comput. Phys. 229 (5) (2010) 3250–3275.
[34] J. S. Sachdev, C. P. T. Groth, J. J. Gottlieb, A parallel solution-adaptive scheme for predicting multi-phase core flows in solid propellant rocket motors, Int. J. Comput. Fluid Dyn. 19 (2) (2005) 159–177.
[35] X. Gao, C. P. T. Groth, A parallel adaptive mesh refinement algorithm for predicting turbulent non-premixed combusting flows, Int. J. Comput. Fluid Dyn. 20 (5) (2006) 349–357.
[36] X. Gao, S. A. Northrup, C. P. T. Groth, Parallel solution-adaptive method for two-dimensional non-premixed combusting flows, Prog. Comput. Fluid Dyn. 11 (2) (2011) 76–95.
[37] M. J. Williamschen, C. P. T. Groth, Parallel anisotropic block-based adaptive mesh refinement algorithm for three-dimensional flows, Paper 2013-2442, AIAA (June 2013).
[38] R. S. Rogallo, Numerical experiments in homogeneous turbulence, Technical Memorandum 81315, NASA (September 1981).